Applied Catalysis B: Environmental 90 (2009) 10–17

Contents lists available at ScienceDirect

Applied Catalysis B: Environmental

journal homepage: www.elsevier.com/locate/apcatb

An investigation of CuO/Fe_2O_3 catalysts for the gas-phase oxidation of ethanol

Guy Litt, Catherine Almquist *

Department of Paper and Chemical Engineering, Miami University, 064J Engineering Building, Oxford, OH 45056, USA

ARTICLE INFO

Article history:
Received 24 July 2008
Received in revised form 30 January 2009
Accepted 4 February 2009
Available online 12 February 2009

Keywords:
Ethanol
CuO/Fe_2O_3 catalysts
Catalytic oxidation

ABSTRACT

The catalytic oxidation of ethanol vapor over CuO/Fe_2O_3 catalysts was investigated. The catalysts were prepared by two different methods: (1) thermal decomposition and (2) flame-aerosol methods. The effects of the catalyst synthesis method and CuO loading on catalyst properties and performance were assessed. The Cu/Fe mass ratio in the catalysts varied from 0 to 0.05 for both synthesis methods used in this study. Catalysts containing a Cu/Fe mass ratio = 1 and pure CuO were also prepared using the thermal decomposition method. The catalysts were characterized for physical and chemical properties via XRD, SEM, TEM, BET surface area analyses, Raman spectroscopy, and TPR. The catalytic activity for the gas-phase oxidation of ethanol was investigated at temperatures ranging from 100 °C to 300 °C. Our experimental results show that the flame synthesized catalysts have higher catalytic activity than thermal decomposition catalysts of similar compositions. The probable reasons for higher activity in the flame-aerosol catalysts are higher surface area and morphological differences.

1. Introduction

The production of ethanol as a biofuel has increased greatly over the past decade due to both environmental and economical reasons. In addition, the United States Environmental Protection Agency (US EPA) established the Renewable Fuel Standard Program, which requires that a minimum volume of renewable fuels be blended with petroleum-based fuels for motor vehicles [1]. With the increased production and use of ethanol, the need for emissions control from production and blending facilities have also increased.

The motivation for this study was to investigate a relatively low-cost catalyst for the vapor-phase oxidation of volatile organic compounds (VOCs). Ethanol is the VOC that was selected for this study. Typically, catalysts containing precious metals are used for the catalytic oxidation of VOCs, and they are commercially available (e.g. http://www.tanaka.co.jp/products-e/products1/f_2.html). They are used for emission controls in industry and transportation. However, the precious metals, which may include platinum, palladium, or gold, add cost to the catalyst. Therefore, there is potential to decrease the cost of the catalyst by developing a catalyst that can be made from less expensive raw materials.

For this study, a mixed metal oxide catalyst, copper oxide/iron oxide (CuO/Fe_2O_3) was selected as a potential VOC oxidation catalyst. This catalyst system has been studied for carbon monoxide (CO) oxidation [2–6], hydrogen production reactions [7,8], water–gas shift reactions [9], peroxide decomposition reactions [10,11], and organic oxidation reactions [12–17]. The published literature provided support for selecting the mixed metal oxide catalyst, CuO/Fe_2O_3. For example, Cheng et al. [3] and Cao et al. [4] found that the catalytic activity of CuO/Fe_2O_3 catalysts for CO oxidation was strongly related to the Cu:Fe molar ratios and to specific surface area, among other properties. El-Shobaky and Fahmy [5] compared the catalytic activity of CuO, Fe_2O_3, and the mixed oxides CuO/Fe_2O_3 supported on cordierite for CO oxidation, and they found that the mixed metal oxide catalyst had higher activity than either CuO or Fe_2O_3 alone. They attributed the enhanced catalytic activity of the mixed oxides to the formation of iron cuprate (Fe_2CuO_4) on its surface. Also supporting the enhanced catalytic performance of mixed oxides was Shaheen [10], who attributed the increased catalytic activity of cobalt and manganese doped Fe_2O_3 over pure Fe_2O_3 to changes in oxidation state at surface-active sites.

The mechanism by which metal oxides catalytically enhance the oxidation of alcohol vapors was studied by Kulkarni and Wachs [12]. They found that isopropanol oxidation on CuO yielded primarily redox products (dehydrogenation to acetone), whereas that on Fe_2O_3 yielded both redox products and acidic products (dehydration to propylene). Kovalenko et al. [15] and Minico et al. [16] investigated the oxidation of ethanol on SnO_2/Fe_2O_3 and Au/Fe_2O_3, respectively. In both studies, the predominant partial oxidation product was the dehydrogenation product, acetaldehyde.

The catalyst synthesis method can affect the catalyst properties, including surface area, morphology, crystallinity, and dispersion and interaction of active sites and dopant metals on the catalyst

* Corresponding author.
E-mail address: almquic@muohio.edu (C. Almquist).

0926-3373/$ – see front matter © 2009 Elsevier B.V. All rights reserved.
doi:10.1016/j.apcatb.2009.02.001

surface. Dong et al. [18] investigated the dispersion and reduction behaviors of CuO on Fe_2O_3 on catalysts prepared by the wet-incipient method. They found that the dispersion capacity of CuO on Fe_2O_3 is 13.7 Cu^{2+}/nm^2 and that heat (calcination) influences the interaction between CuO and Fe_2O_3 [18]. Shaheen and Ali [19] investigated the role of temperature on catalysts synthesized by thermal decomposition of copper and iron nitrates in varying ratios. Two observations in their study that are relevant to this study are (1) iron-rich catalysts (1Cu–3Fe) showed no CuO phase on XRD analyses, and (2) the increased catalytic activity of mixed oxides compared to CuO or Fe_2O_3 alone suggest the creation of (Cu^{x+}–Fe^{y+}) ion pairs at the catalyst surface, which may act as active sites [19].

The synthesis method most used by researchers to prepare CuO/Fe_2O_3 catalysts is the coprecipitation method. In this method, iron nitrate and copper nitrate solutions are mixed at the desired iron-to-copper ratios, the pH is adjusted with caustic to greater than 9 to effect precipitation, and the precipitate is collected by filtration. The precipitate is subsequently washed, dried, and calcined. Other methods used to prepare CuO/Fe_2O_3 catalysts include thermal decomposition of metal carbonates and/or nitrates, sol–gel, and combustion processes. In a flame-aerosol method, solutions of copper and iron precursors are prepared, aerosolized, and directed through a flame. This method results in spherical nanostructured mixed oxide particles. However, the morphology and metal oxide distribution within the particles prepared by the flame-aerosol method are dependent upon flame temperature, residence time, aerosolizer design, as well as the metal oxide precursors and carrier liquids [20,21]. In studies by Kumar et al. [22] and Stark et al. [23], the activities of flame-aerosol catalysts were compared to those of wet-incipient catalysts, and in both studies, the flame-aerosol catalysts had higher activity, presumably due to higher surface area and more uniform distribution of dopant on the catalyst support surface [22,23].

In this study, CuO/Fe_2O_3 catalysts were prepared by two methods: (1) thermal decomposition of Cu and Fe nitrates and (2) the flame-aerosol method. For both methods, catalysts containing Cu/Fe mass ratios of 0, 0.01, and 0.05 were prepared for comparison. In addition, catalysts containing a Cu/Fe mass ratio of 1 and pure CuO were prepared using thermal decomposition of nitrate solutions. The physical and chemical properties of the catalysts were investigated, and the catalytic activities of the catalysts for the gas-phase oxidation of ethanol were assessed and compared.

2. Experimental

2.1. Catalyst preparation

The catalysts were prepared by two methods: (1) thermal decomposition of aqueous nitrate solutions, and (2) the flame-aerosol method. Each method is described below:

2.1.1. Thermal decomposition

Aqueous solutions of $Cu(NO_3)_2{\cdot}H_2O$ and $Fe(NO_3)_3{\cdot}9H_2O$ (Aldrich) were prepared in deionized water with Cu/Fe mass ratios of 1 g Cu/g Fe (C50), 0.05 g Cu/g Fe (C5), 0.01 g Cu/g Fe (C1) and 0 g Cu/g Fe (C0). In addition, a solution containing only $Cu(NO_3)_2{\cdot}H_2O$ was prepared to synthesize a catalyst of pure CuO. The solutions were sonicated for 15 min using a Branson sonicator to assist in dissolving and mixing the nitrates. The samples were dried in an oven at 104 °C for 40 h, having been stirred after 18 h. After drying, the samples were ground with a mortar and pestle, and then calcined at 400 °C in air for nearly 17 h. Again, the samples were ground with mortar and pestle and stored in vials until used.

Fig. 1a shows a cartoon of how, hypothetically, catalysts synthesized by thermal decomposition would be formed. The goal of the cartoon is to show that CuO is expected to be distributed uniformly throughout the Fe_2O_3 crystal structure.

2.1.2. Flame-aerosol method

In the flame-aerosol method, the nitrate solutions were prepared as described above with Cu to Fe mass ratios of 0.05 g Cu/g Fe (F5), 0.01 g Cu/g Fe (F1) and 0 g Cu/g Fe (F0). The solutions were aerosolized with a medical nebulizer and directed via an air stream through a diffusion flame. Fig. 1b shows a cartoon of how, hypothetically, the catalyst particles would form in the flame-aerosol method. Since the melting points of Fe_2O_3 and CuO are 1565 °C and 1326 °C (www.micrometals.com), respectively, the Fe_2O_3 particles would nucleate first, and the CuO would deposit and/or condense onto the Fe_2O_3 particles as they further cool. Thus, the CuO is expected to be more concentrated on the outside of the catalyst particles than on the inside.

A diffusion burner containing three concentric stainless steel tubes was used to create a flame. The outer tube carried methane at 0.29 lpm and the middle tube delivered oxygen at 1.4 lpm to maintain the flame. Air containing the aerosolized precursor solution was delivered to the flame at 1.8 lpm in which the

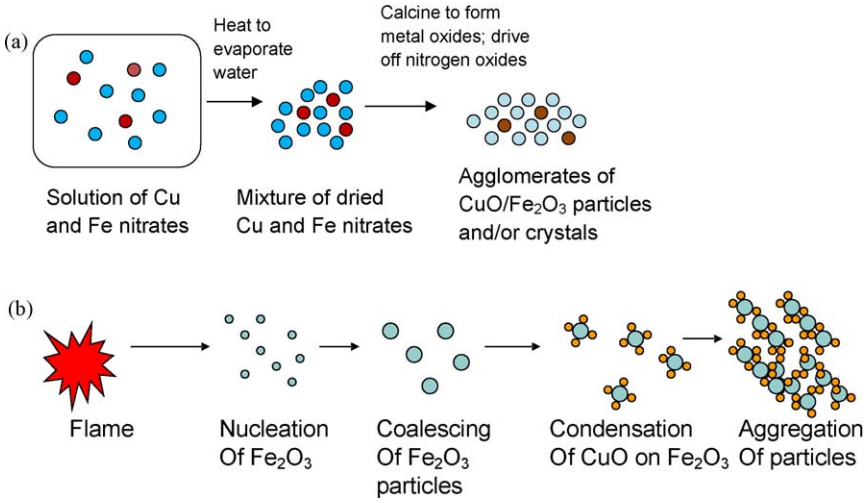

Fig. 1. Hypothesized scheme for the distribution of CuO in Fe_2O_3 at low CuO loadings in (a) thermal decomposition catalysts and (b) flame-aerosol catalysts.

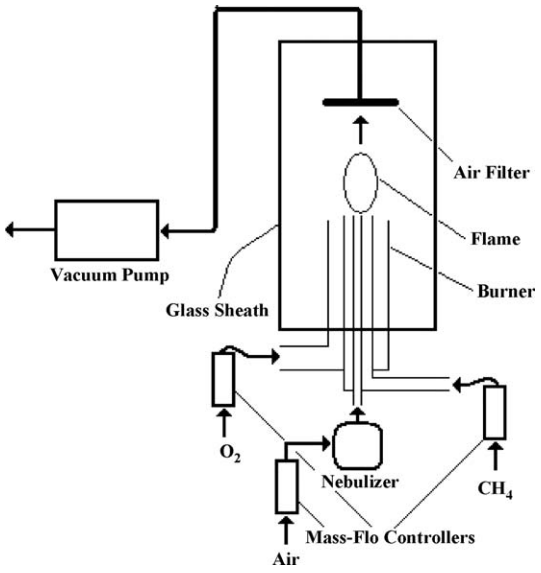

Fig. 2. Schematic of flame-aerosol catalyst synthesis test system.

aerosolized Cu and Fe nitrate-containing particles were thermally decomposed to nanostructured metal oxide particles. The nanostructured oxide particles were collected on a Whatman 47 mm quartz fiber air filter that was positioned 8 in. directly above the diffusion burner. The filter was connected to a vacuum pump to assist in particle collection on the filter. The diffusion burner and air filter were contained in a glass sheath, which protected the flame and the particles from air movement within the chemical fume hood. A schematic of the diffusion burner and test system for the flame-aerosol method is shown in Fig. 2.

2.2. Catalyst characterization

The catalysts were characterized using X-ray diffraction (XRD), Raman spectroscopy, BET surface area, scanning electron microscopy (SEM), transmission electron microscopy (TEM), energy dispersive spectroscopy (EDS), and temperature-programmed reduction (TPR). Each catalyst characterization method is described below.

2.2.1. X-ray diffraction (XRD)

The crystallinity of each catalyst sample was characterized with a Scintag X1 Powder XRD equipped with a Cu Kα source. The Bragg angles used to obtain XRD spectra of the catalysts ranged from $20^\circ < 2\theta < 60^\circ$ and data was acquired at a scanning rate of .04 degrees/s and step size of .02 degrees.

2.2.2. BET surface area

The specific surface area of each catalyst was measured by nitrogen adsorption at 77 K using the Brunauer Emmett and Teller (BET) surface analysis method with a Beckman Coulter SA 3100 Surface Analyzer. The catalyst samples were out-gassed with a helium purge at 125 °C for 45 min prior to each analysis.

2.2.3. Scanning electron microscopy (SEM) and energy dispersive spectroscopy (EDS)

A Zeiss Supra 35 VP was used to capture SEM images of the catalyst samples at magnifications ranging from 77× to 12,000×. The EDS microanalysis was operated at 20 kV for 200 live seconds on each sample, measuring the percentage compositions of CuO and Fe_2O_3 by EDAX ZAF standardless quantification of oxides.

2.2.4. Transmission electron microscopy (TEM)

TEM micrographs were obtained for the catalysts using a Zeiss 10C TEM operating at 100 kV. The catalyst powders were dispersed in 2-propanol, and the mixtures were applied to carbon backed TEM grids prior to the analyses.

2.2.5. Raman spectroscopy

Raman spectra were collected under ambient conditions using a Renishaw 2000 confocal Raman microprobe. Samples were excited with a HeNe (632 nm) laser. This source was focused onto the sample, producing an approximate beam diameter of 2 mm at the sample. Power at the sample did not exceed 6 mW. Spectra were collected at 4 cm^{-1} resolution and represent the average of five individual scans. The integration time for each spectral element was 30 s. The Raman analyses provide some insight to variations in bond vibrational energy as a function of CuO loading on Fe_2O_3.

2.2.6. Temperature-programmed reduction (TPR)

Temperature-programmed reduction with hydrogen was performed on the catalysts using a Micrometric Autochem 2920 instrument. The catalyst (74 mg) was charged in a stainless steel U tube reactor, and a flow of hydrogen was directed through the catalyst at temperatures ranging from 40 °C to 800 °C. TPR provides insight into the effects of CuO/Fe_2O_3 interactions on the redox properties of the catalysts.

2.3. Catalyst performance

The oxidation of ethanol vapor was used to assess the activity of the catalysts. A schematic of the test system is provided in Fig. 3. The reaction was carried out in a Lindbergh/Blue tube furnace reactor, with a 55 cm long stainless steel tube (0.635 cm OD and 0.09 cm wall thickness). The center of the steel tube contained 50 mg catalyst enclosed in a bed of quartz wool. Ethanol vapor was generated at a constant 8000 ppm in 20 ml/min using a diffusion cell as the vapor generator and a mass flow controller to control the gas flow. The effluent stream from the tube reactor was analyzed using a thermal conductivity detector (TCD) with on-line gas injections on an Agilent Technologies 6890N gas chromatograph. A bypass stream was included around the tube reactor to assess the inlet ethanol concentrations. The temperature of the tube reactor was set to 100 °C initially, followed by a setting of 150 °C. Further temperature settings for the reaction increased at 25 °C increments.

3. Results and discussion

Table 1 provides the BET surface area of each catalyst and their nominal and EDS-obtained Cu/Fe mass ratios. Noted is that the BET surface areas of the flame-aerosol catalysts are higher than those of the thermal decomposition catalysts by a factor of approximately two. This is likely due to differences in the morphologies of the catalysts as a result of their synthesis methods. As suggested by Fig. 1a and b, the calcination of the thermal decomposition catalysts can create agglomerates of closely packed and even fused

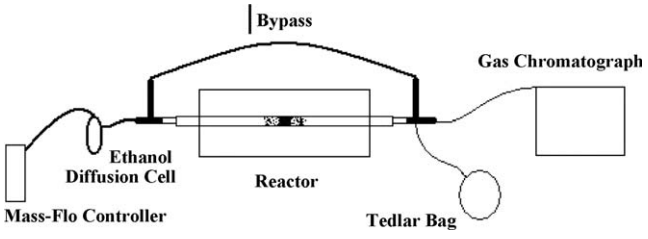

Fig. 3. Schematic of catalytic oxidation test system.

Table 1
Catalyst composition and surface area.

Catalyst	Nominal (EDS) Cu/Fe mass ratio	BET surface area (m^2/g)
C0	0 (0)	25
C1	0.01 (0.011)	29
C5	0.05 (0.041)	26
C50	1.0 (0.83)	29
CuO	Pure CuO	20
F0	0 (0)	37
F1	0.01 (0.027)	41
F5	0.05 (0.035)	54

particles, which can blind or block accessibility to catalyst surfaces. In contrast, however, the flame synthesized catalysts form relatively open fractal structures, which allow accessibility to the surfaces of the catalyst particles. This reasoning is supported by SEM micrographs of the catalysts, as discussed below.

SEM micrographs of the thermal decomposition and flame-aerosol catalysts are shown in Fig. 4a and b, respectively. Noted is that the thermal decomposition catalysts form agglomerates of closely packed, if not fused, particles. The agglomerates can be quite large, up to 10 μm. In contrast, Fig. 4b clearly shows the poly-dispersed, spherical nature of the flame-aerosol catalysts, with spherical particles ranging up to 2 μm in size.

The TEM micrographs of thermal decomposition catalysts and flame-aerosol catalysts are shown in Fig. 5a and b, respectively. Note that the TEM micrographs show catalyst samples at more than 30 times higher magnification than the SEM micrographs, and so by the nature of the analytical method, the smaller particles (<100 nm) are pictured via TEM. Fig. 5a shows that the thermal decomposition catalysts have a relatively uniform particle size distribution of approximately 15 nm. These particles are likely representative of those seen coating the outside of the larger agglomerates or crystals in the SEM micrographs (Fig. 4a). In contrast, the flame-aerosol catalysts (Fig. 5b) are poly-dispersed spherical nanoparticles with most particles <10 nm, which are too small to be clearly observed with the TEM used in this study. Although there are a few large particles (>50 nm), the specific surface area is dominated by the smaller particles of the flame-aerosol catalysts. The particles form relatively open agglomerate structures of particles, thus allowing accessibility to the surfaces of the primary catalyst particles. The wide particle size distribution for the flame-aerosol method is likely due to the wide particle size distribution of the aerosol provided by the medical nebulizer to the diffusion flame. A narrower particle size distribution resulting from the flame-aerosol catalysts could be achieved by using an

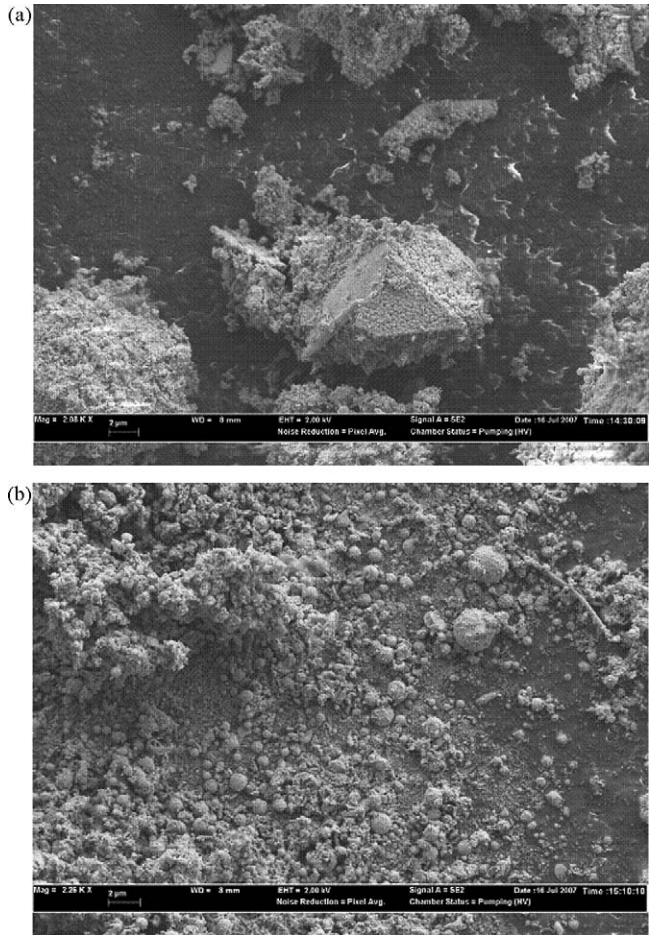

Fig. 4. SEM micrographs for (a) thermal decomposition catalysts (C1) and (b) flame-aerosol catalysts (F1).

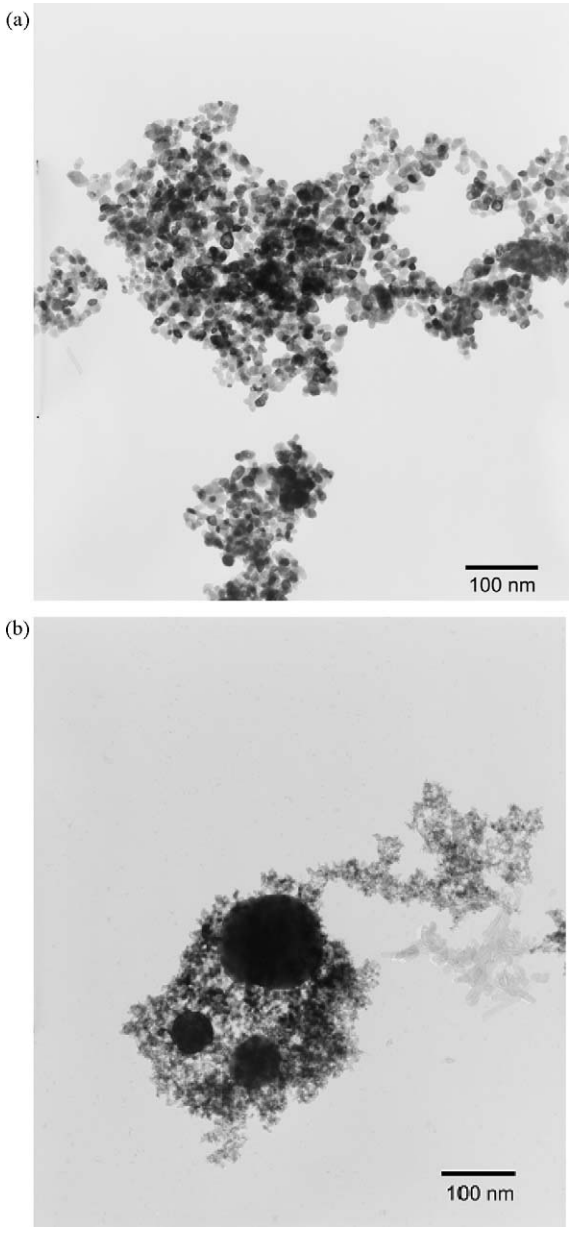

Fig. 5. TEM micrographs of (a) thermal decomposition catalysts (C1) and (b) flame-aerosol catalysts (F1).

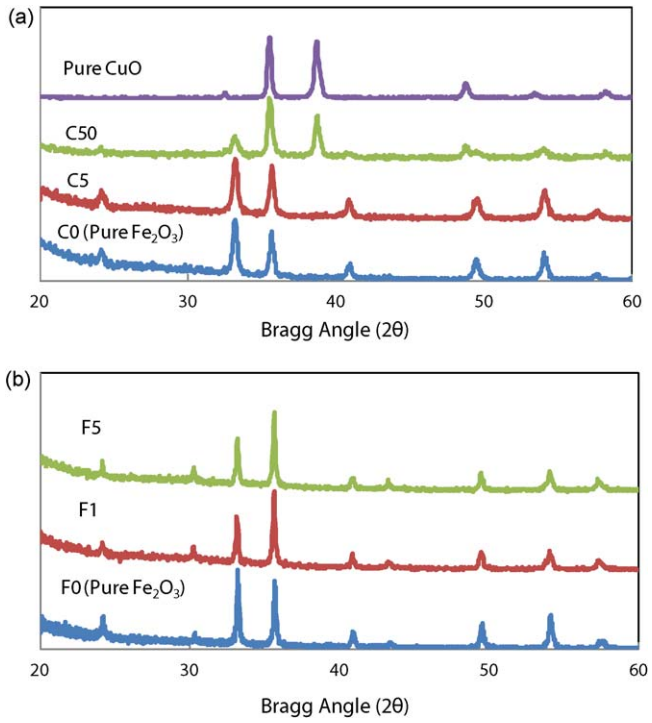

Fig. 6. XRD spectra of (a) thermal decomposition catalysts and (b) flame-aerosol catalysts.

aerosolizer that produced a narrower particle size distribution. Different precursors and modifications to the flame-aerosol test system also could result in a more uniform particle size distribution.

The XRD spectra of the catalysts are shown in Fig. 6a and b for the thermal decomposition catalysts and flame-aerosol catalysts, respectively. Noted is that there are no observable CuO characteristics in any of the catalysts containing Cu/Fe mass ratios $\leq$0.05 and that the Fe_2O_3 crystal structure is rhombohedral hematite [4]. Also noted from Fig. 6a is that both cuprite (CuO) and Fe_2O_3 characteristics are observable in catalyst C50. Fe_2CuO_4 was not observed in any of the XRD spectra, which is in contrast to the observations of El-Shobaky and Fahmy [5].

Raman analyses of the thermal decomposition catalysts and for the flame-aerosol catalysts are shown in Figs. 7 and 8, respectively. The Raman spectra support that the structure of Fe_2O_3 is hematite [24–27], with predominant peaks at wavenumbers (vibrational mode assignments for Fe–O) of approximately 224 cm^{-1} (A_{1g}), 290 cm^{-1} (E_g) and 410 cm^{-1} (E_g) [24,26,27]. Noted is that as CuO loading increases, the predominant Raman peaks of Fe_2O_3 red shift (shift toward lower wavenumbers, hence lower energy), as shown in Figs. 7b and 8b. Fig. 9 shows the red shift in Raman wavenumber for the three predominant peaks in Fe_2O_3. As the Cu/Fe mass ratio increases from 0 to 0.05, the wavenumber red shifts by up to 5 cm^{-1}, with only slightly more shift in the flame-aerosol catalysts than the thermal decomposition catalysts. Shifts in Raman peaks can be due to effects of particle size and/or due to strains and defects in the crystal structure [28]. In this study, the red shift in wavenumber is attributed to changes in surface strain and defects caused by the incorporation of CuO into the Fe_2O_3 crystal structure.

TPR analyses of the catalysts are shown in Fig. 10a and b for the thermal decomposition and flame-aerosol catalysts, respectively. Noted is that in both Fig. 10a and b, the pure hematite Fe_2O_3 catalysts show a small peak at ~370 °C, which can be attributed to the reduction of Fe_2O_3 to Fe_3O_4 [4,16,29], and a large broad peak with a maximum greater than 600 °C, which can be attributed to further reduction to FeO [4,16,29]. This is supported by the results

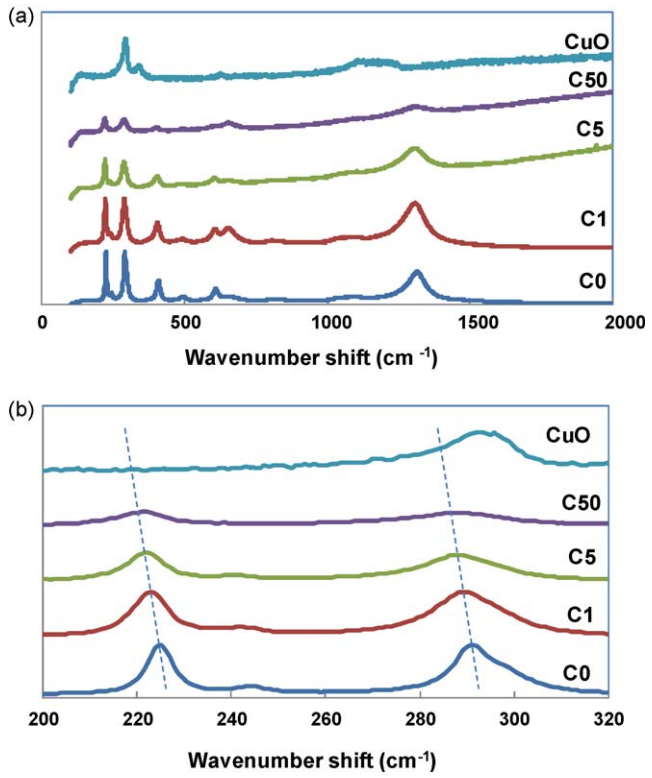

Fig. 7. Raman spectroscopy analyses of thermal decomposition catalysts. (a) Wavenumber range from 200 cm^{-1} to 2000 cm^{-1} and (b) wavenumber range from 200 cm^{-1} to 320 cm^{-1} showing a blue shift in the Fe_2O_3 peaks as Cu/Fe mass ratio increases.

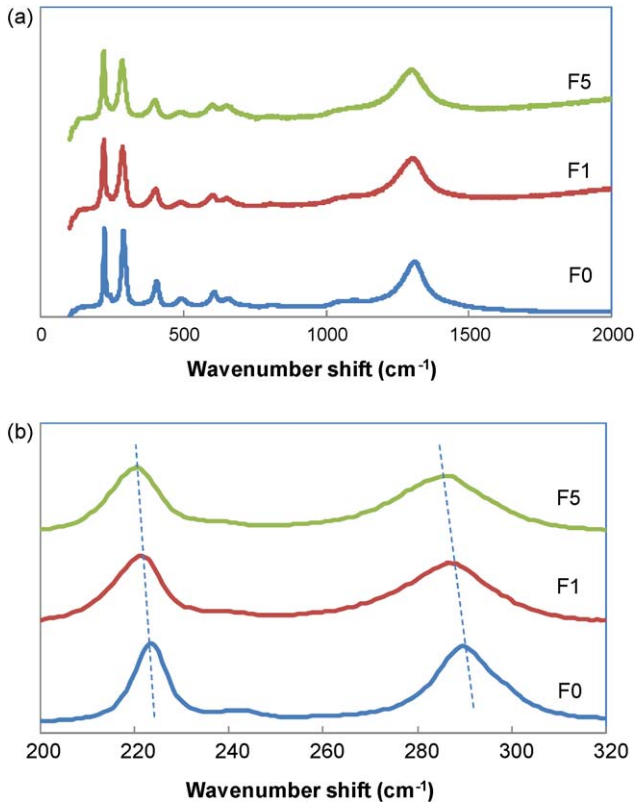

Fig. 8. Raman spectroscopy analyses of flame-aerosol catalysts. (a) Wavenumber range from 200 cm^{-1} to 2000 cm^{-1} and (b) wavenumber range from 200 cm^{-1} to 320 cm^{-1} showing a blue shift in the Fe_2O_3 peaks as Cu/Fe mass ratio increases.

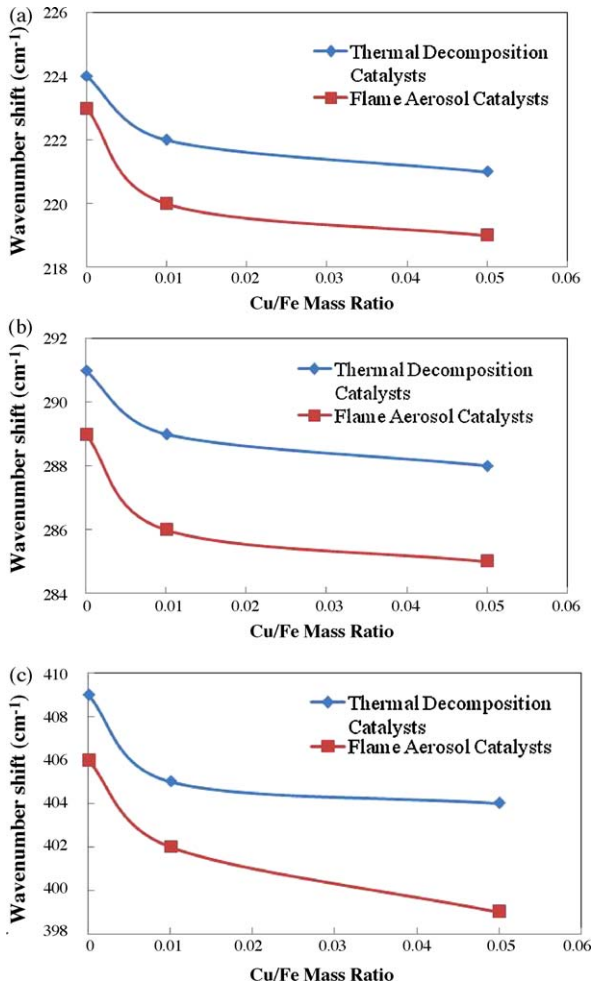

Fig. 9. Wavenumber shifts for predominant hematite Fe_2O_3 Raman peaks: (a) 224 cm^{-1}; (b) 290 cm^{-1}; (c) 409 cm^{-1}.

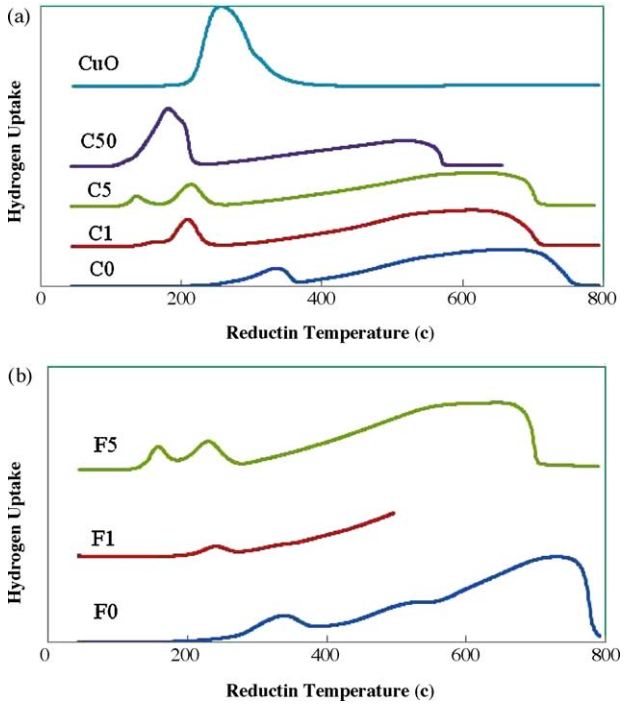

Fig. 10. Temperature-programmed reduction (TPR) spectra of (a) thermal decomposition catalysts and (b) flame-aerosol catalysts.

of Minicio et al. [16], who also showed similar TPR spectra for hematite. Fig. 10a and b also shows that the presence of CuO on Fe_2O_3 decreases the temperature at which reduction occurs, as indicated by the shift in the first peak (hydrogen uptake) to lower temperatures. Noted, too, in Fig. 10a is that the pure CuO catalyst has one large peak at approximately 250 °C, and that the presence of Fe_2O_3 (catalyst C50) shifts that peak to lower temperatures. Minico et al. reported similar TPR results with gold (Au)-doped Fe_2O_3 (Au/Fe_2O_3) catalysts, and they attributed the lower reduction temperatures to the effect of Au and Fe_2O_3 interactions on lattice oxygen mobility [16]. By analogy, it is likely that the presence of Cu decreases the strength of nearby Fe–O bonds, thus increasing the mobility of lattice oxygen and facilitating redox reactions on the catalyst surface.

Fig. 11a–c compares catalysts of similar composition but prepared by different methods. Noted is that in all comparisons, the catalysts' TPR spectra are similar, but the thermal decomposition catalysts have surface sites that are reduced at slightly lower temperatures than the flame-aerosol catalysts. Considering the synthesis methods and respective morphologies of catalysts prepared by those methods (Fig. 1a and b), the thermal decomposition catalysts would have the more uniform distribution of Cu within the Fe_2O_3 structure, whereas the Cu is hypothesized to be more concentrated on the surface of flame-aerosol catalysts. The differences in morphology and Cu distribution in the Fe_2O_3 crystal structure are possible reasons for differences observed in Fig. 11a–c.

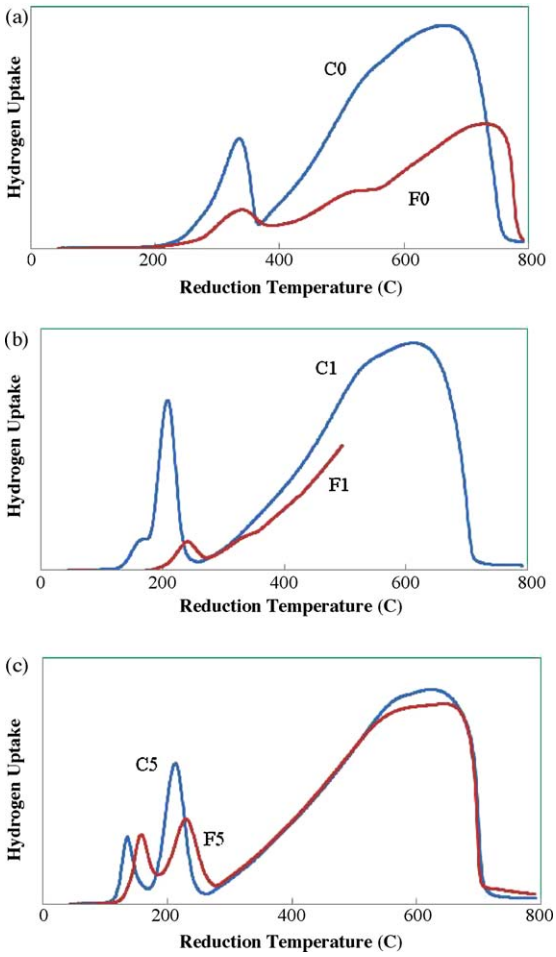

Fig. 11. Comparison of thermal decomposition and flame-aerosol catalysts of similar composition.

3.1. Catalyst performance

The results from the catalysis experiments indicate that the presence of CuO on Fe_2O_3 enhances the activity of the catalyst, as shown in Fig. 12a and b. This supports the observations of El-Shobaky and Fahmy [5], who also found that the mixed oxides had higher activity than Fe_2O_3 alone. For the thermal decomposition catalysts (Fig. 12a), the activity of the catalyst increased up to a Cu/Fe mass ratio of 1.0. Pure CuO had relatively poor activity for the oxidation of ethanol compared to the CuO/Fe_2O_3 composite catalysts, likely due to its very low surface area (2 m^2/g) and its surface characteristics. For the flame-aerosol catalysts, the presence of CuO on Fe_2O_3 enhances the activity of the catalysts; however, the effect of CuO loading is much less apparent than with the thermal decomposition catalysts.

According to Vedrine et al. [30], the Mars-van-Krevelen mechanism is a probable mechanism for many catalytic oxidation reactions of volatile organic compounds over mixed metal oxide catalysts. The Mars-van Krevelen mechanism requires that a lattice oxygen from the catalyst surface is involved in the reaction. Therefore, high lattice oxygen mobility is favorable. The presence of Cu in Fe_2O_3 likely increases the lattice oxygen mobility, as implied in both Raman and TPR analyses, and so Cu also enhances the catalytic activity of Fe_2O_3.

In all cases, the flame-aerosol catalysts had higher activity than the thermal decomposition catalysts of similar composition. Fig. 13a–c shows a comparison of CuO/Fe_2O_3 catalysts of similar composition but prepared by two different methods: thermal decomposition (solid markers) and flame-aerosol (open markers) methods. Except for the BET surface area and morphology (as shown by SEM micrographs in Fig. 4a and b), the properties of the catalysts prepared by the two methods are similar for similar composition. Therefore, the higher surface area and morphology of the flame-aerosol catalysts are the likely reasons for their apparent greater activity over the thermal decomposition catalysts of similar composition.

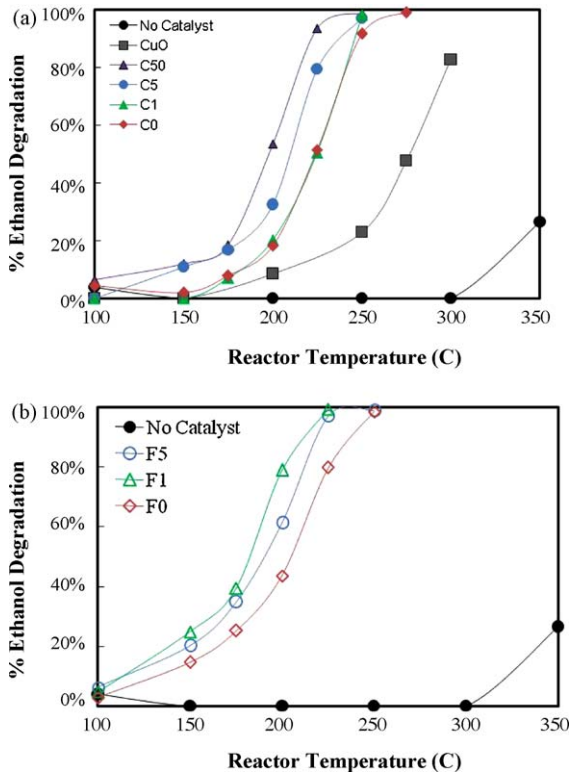

Fig. 12. Ethanol conversion as a function of reactor temperature for (a) thermal decomposition catalysts and (b) flame-aerosol catalysts.

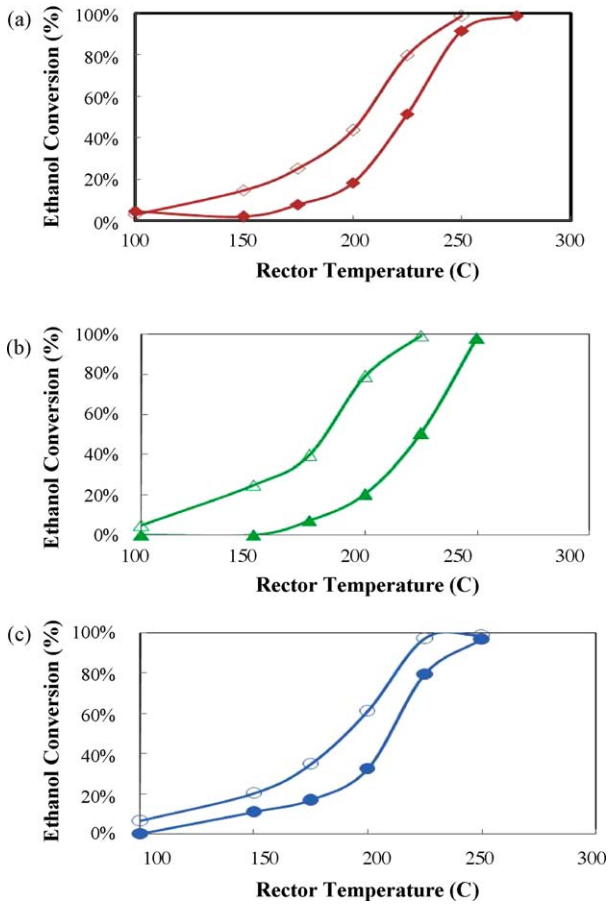

Fig. 13. Comparison of catalyst performance of flame-aerosol catalysts (open markers) and thermal decomposition catalysts (closed markers) for catalysts with Cu/Fe mass ratio = (a) 0, (b) 0.01 and (c) 0.05.

From the data used in Fig. 13a–c, the apparent activation energies were calculated to be 63 ± 5 kJ/mol for flame synthesized catalysts and 80 ± 14 kJ/mol for thermal decomposition catalysts, suggesting that morphology and surface properties of flame-aerosol catalysts lead to higher activity for ethanol oxidation than the thermal decomposition catalysts.

The predominant partial oxidation product of ethanol over the CuO/Fe_2O_3 catalysts was acetaldehyde, as confirmed by mass spectrometry in this study and supported by published literature [15–17]. The presence of acetaldehyde was most notable at low reaction temperatures, hence, low ethanol conversions. At higher reaction temperatures, and hence, at higher ethanol conversions, the acetaldehyde, as well as other observable partial oxidation products, were further oxidized, presumably to CO_2. The other partial oxidation products that were observed at low reaction temperatures were neither identified nor quantified in this study, because they were present in concentrations that were factors of approximately 10 to 50 lower than that of acetaldehyde. Kovalenko et al. [15] also found that acetaldehyde was the predominant partial oxidation product of ethanol over SnO_2/Fe_2O_3 catalysts. In their study, the other partial oxidation products were identified as ethylene, ethyl acetate, diethyl ether, acetic acid and acetone. However, with increasing Fe_2O_3 content in the catalyst, the conversion of ethanol to acetaldehyde and CO_2 increased while ethanol conversion to all other partial oxidation products decreased under similar test conditions [15].

4. Conclusion

Our experimental results showed that catalysts having similar compositions have similar properties, even though they were prepared by two different methods, the thermal decomposition and flame-aerosol methods. Two exceptions to their similarities are surface area and morphology. The flame synthesized catalysts had higher surface area and more open-structured agglomerates than the thermal decomposition catalysts. The catalytic activities of the flame synthesized catalysts were also higher than those of the thermal decomposition catalysts of similar compositions. Possible reasons for the higher activity of the flame-aerosol catalysts include higher surface area and more accessibility to surface-active sites on the catalysts.

In this study, a wide particle size distribution was observed in the flame-aerosol catalysts. A narrower particle size distribution could be realized by using an aerosolizer that generates an aerosol with a narrower particle size distribution. The precursors used for catalysts synthesis also may make significant differences in catalyst particle morphology and size distribution.

The mixed metal oxide (CuO/Fe_2O_3) catalysts were more active than either pure Fe_2O_3 or pure CuO catalysts, likely due to greater lattice oxygen mobility in the mixed oxide catalysts. The predominant partial oxidation product observed in this study was acetaldehyde, suggesting that redox active sites were predominant on the CuO/Fe_2O_3 catalysts used in this study.

Acknowledgements

The authors thank the following people for their support in this research: Dr. Richard Edelmann (Miami University) for TEM, SEM, and EDS analyses; Dr. Andre Sommer (Miami University) for Raman Spectroscopy and FTIR analyses of the catalysts; Drs. Venu Gopal and E. Sahle-Demessie (US EPA, Cincinnati) for TPR analyses of the catalysts.

References

[1] Renewable Fuel Standard Program. United States Environmental Protection Agency. 4 September 2007. US EPA. 18 October 2007, http://www.epa.gov/otaq/renewablefuels/.
[2] H.G. El-Shobaky, M.M. Mokhtar, Appl. Surf. Sci. 253 (2007) 9407.
[3] T. Cheng, Z. Fang, Q. Hu, K. Han, X. Yang, Y. Zhang, Catal. Commun. 8 (2007) 1167.
[4] J.-L. Cao, Y. Wang, X.-L. Yu, S.-R. Wang, S.-H. Wu, Z.-Y. Yuan, Appl. Catal. B 79 (2008) 26.
[5] H.G. El-Shobaky, Y.M. Fahmy, Mater. Res. Bull. 41 (2006) 1701.
[6] X. Zheng, S. Wang, S. Wang, S. Zhang, W. Huang, S. Wu, Catal. Commun. 5 (2004) 729.
[7] W. Wang, Z. Wang, Y. Ding, J. Xi, G. Lu, Catal. Lett. 81 (2002) 63.
[8] M. Scariot, S.P. Francisco, M. Jordao, D. Zanchet, M. Logli, V.P. Vicentini, Catal. Today 133–135 (2008) 174.
[9] M.V. Twigg, Catalyst Handbook, 2nd ed., Manson Publishing, London, 1989, p. 284.
[10] W.M. Shaheen, Mater. Chem. Phys. 101 (2007) 182.
[11] J.A. Melero, G. Calleja, F. Martinez, R. Molina, Catal. Commun. 7 (2006) 478.
[12] D. Kulkarni, I.E. Wachs, Appl. Catal. A 237 (2002) 121.
[13] T. Garcia, B. Solsona, S.H. Taylor, Appl. Catal. B 66 (2006) 92.
[14] B.N.T. Nguyen, C.A. Leclerc, J. Power Sources 163 (2007) 623.
[15] V.V. Kovalenko, M.N. Rumyantseva, A.M. Gaskov, E.V. Makshina, V.V. Yushchenko, I.I. Ivanova, A. Ponzoni, G. Faglia, E. Comini, Inorg. Mater. 42 (2006) 1088.
[16] S. Minico, S. Scire, C. Crisafulli, R. Maggiore, S. Galvagno, Appl. Catal. B 28 (2000) 245.
[17] Z.R. Ismagilov, N.M. Dobrynkin, V.V. Popovskii, React. Kinet. Catal. Lett. 1 (1979) 55.
[18] L. Dong, Z. Liu, Y. Hu, B. Xu, Y. Chen, J. Chem. Soc., Faraday Trans. 94 (1998) 3033.
[19] W.M. Shaheen, A.A. Ali, Intern. J. Inorg. Mater. 3 (2001) 1073.
[20] R. Jossen, S.E. Pratsinis, W.J. Stark, L. Madler, J. Am. Ceram. Soc. 88 (6) (2005) 1388.
[21] W.J. Stark, L. Madler, M. Maciejewski, S.E. Pratsinis, A. Baiker, Chem. Commun. 5 (2003) 588.
[22] V. Kumar, N. Lee, C.L.B. Almquist, Appl. Catal. B 69 (2006) 101.
[23] W.J. Stark, K. Wegner, S.E. Pratsinis, A. Baiker, J. Catal. 197 (2001) 182.
[24] D. Bersani, P.P. Lottici, A. Montenero, J. Raman Spectrosc. 30 (1999) 355.
[25] J.A. Glasscock, P.R.F. Barnes, I.C. Plumb, A. Bendavid, P.J. Martin, Thin Solid Films 516 (2008) 1716.
[26] W. Chen, X. Pan, Z. Bao, J. Am. Chem. Soc. 129 (2007) 7421.
[27] J. Wang, W.B. White, J.H. Adair, J. Am. Ceram. Soc. 88 (12) (2005) 3449.
[28] C.Y. Xu, P.X. Zhang, L. Yan, J. Raman Spectrosc. 32 (2001) 862.
[29] C. Messi, P. Carniti, A. Gervasini, J. Therm. Anal. Calorim. 91 (2008) 93.
[30] J.C. Vedrine, G. Coudurier, J-M.M. Millet, Catal. Today 33 (1997) 3.